Title: The double-edged role of nitric oxide drives predictable microbial community organization according to the microenvironment.

Steven A. Wilbert[1] and Dianne K. Newman[1,2,*]

Contact information:

[1] Division of Biology and Biological Engineering, California Institute of Technology, Pasadena, California, USA, 91125

[2] Division of Geological and Planetary Sciences, California Institute of Technology, Pasadena, California, USA, 91125

[*]**Correspondence:**

Dianne K. Newman

1200 E. California Blvd., Mail code 147-75

Pasadena, CA 91125

Telephone: 626-395-3543

Email: dkn@caltech.edu

Keywords: Polymicrobial communities, metabolism, metabolic cross-feeding, nitric oxide, nitrate, denitrification, spatial organization, microenvironment, oxygen gradients, *Pseudomonas aeruginosa*

Abstract

Microbial assemblages are omnipresent in the biosphere, forming communities on the surfaces of roots, rocks, and within living tissues. These communities can exhibit strikingly beautiful compositional structures, with certain members reproducibly occupying particular spatiotemporal microniches. Yet often, we lack the ability to explain the spatial patterns we see within them. To test the hypothesis that certain spatial patterns in microbial communities may be explained by the exchange of redox-active metabolites whose biological function is sensitive to environmental gradients, here we developed a simple community consisting of synthetic *Pseudomonas aeruginosa* strains with a partitioned denitrification pathway: a strict consumer and strict producer of nitric oxide (NO), a key pathway intermediate. Because NO can be both toxic or beneficial depending on the amount of oxygen present, this system provided an opportunity to investigate whether dynamic oxygen gradients can tune metabolic cross-feeding

in a predictable fashion. Using a combination of genetic analysis, different growth environments and imaging, we show that oxygen availability controls whether NO cross-feeding is commensal or mutually beneficial, and that this organizing principle maps to the microscale. More generally, this work underscores the importance of considering the double-edged roles redox-active metabolites can play in shaping microbial communities.

Introduction

Given the diversity of microbial metabolic strategies and that microbes rarely live alone, the potential for metabolic interactions is vast (Zuñiga et al., 2017). Metabolic interactions can be positive or negative and can have profound effects on the surrounding environment, from contributing to nutrient flux to stimulating the immune system of an infected animal or plant. Therefore, there is an increasing appreciation for the need to characterize and predict such interactions (Widder et al., 2016). Numerous ecological models have been developed to better understand how such interactions influence the growth and subsequent spatial patterning of a community (Goldford et al., 2018; Niehaus et al., 2019; Ratzke et al., 2020). However, these models typically focus on simple growth kinetics involving a shared or exchanged beneficial metabolite and do not consider how changing microenvironments over small spatial scales can influence the initiation and/or quality of interactions dependent upon this metabolite. In particular, dynamic spatiotemporal changes in oxygen availability is a well-documented ecological phenomenon microbes are confronted with (Dal Co et al., 2019; Krichels et al., 2019; Lowery and Ursell, 2019; Stewart et al., 2016), but is often overlooked in these models.

Diffusible, redox-active metabolites, be they organic or inorganic, are particularly interesting to consider in this context, as these molecules' reactivity is highly sensitive to local chemistry. Recent work has called attention to the fact that certain redox-active metabolites have the potential to be both toxic (i.e. generate reactive oxygen species under oxic conditions) or beneficial (i.e. contribute to energy conservation under anoxic conditions), thereby having the potential to play different and dynamic roles in the development of a microbial community (Dahlstrom et al., 2020). Such double-edged effects may be particularly important when the metabolite in question is an intermediate in a common metabolic pathway. For example, if two microbes are reliant on each other for growth due to an intermediate that can be toxic to the producer but is essential for the consumer, it stands to reason that their growth and subsequent environmental impact will depend on microenvironmental conditions that tune the properties of the exchanged intermediate. The potential for variable local interactions due to shifting

environmental gradients would therefore be expected to tune when, where, and how certain microbial interactions would manifest spatiotemporally.

As a step towards testing this general hypothesis, we sought to create a simple synthetic model system in which to explore the effect of the microenvironment on the interactions between two bacterial partners linked via an exchanged redox-active metabolite. Four criteria guided our development of such a system. First, we required that the metabolite be "agathokakological", a word derived from Greek roots meaning "composed of good and evil", in other words, a metabolite that is predictably "double-edged": beneficial or harmful according to its context. Second, we needed to be able to measure and perturb the most important environmental parameter—oxygen—that affects its physiological functions. Third, we aimed to control the production and utilization of this metabolite via the generation of mutant strains from an isogenic background in order to focus strictly on the capacity to make or use it. Finally, we sought a metabolic exchange that is broadly ecologically relevant across many environments.

The exchange of nitric oxide (NO) met all of our criteria. NO is known in both the eukaryotic and microbial worlds as a potent signaling molecule and a highly reactive nitrogen species that can damage a variety of cellular components (Volk et al., 2004). In the absence of oxygen, NO is toxic at high concentrations by antagonizing Fe-S centers and causing DNA damage; yet in the presence of oxygen, much lower levels of NO can be toxic due the generation of peroxynitrite; (Koppenol and Koppenol, 2021; Zumft, 1997). Microbes have numerous mechanisms to deal with low levels of NO toxicity such as flavohemoglobin proteins (Fhp) that can reduce NO to nitrous oxide (N_2O), or mediate its oxidation to nitrate (NO_3^-), depending on the environment (Arai, 2011; Koskenkorva et al., 2008), and other dioxygenases can sequester NO (Sasaki et al., 2016; Yoon et al., 2007). While NO has been studied in detail with respect to these properties, it can also support energy conservation. At the right concentrations, and if a microbe has the requisite machinery to process it, in the absence of oxygen, NO can serve as a terminal electron acceptor (TEA) for anaerobic respiration (Carr et al., 1989; Kalkowski, 1991). Yet as its concentration rises, and if producing cells or neighbors are unable to reduce it to nitrous oxide (N_2O), it reaches toxic levels and leads to local growth inhibition or death (Brunelli et al., 1995; Yu et al., 1999).

NO production is a landmark step in denitrification, where the soluble substrate nitrite (NO_2^-) is reduced to gaseous NO. Denitrification *sensu stricto* plays a critical role in the loss of nitrogen in soils (Fang et al., 2015; Krichels and Yang, 2019; Tian et al., 2019). If an organism contains a full pathway to sequentially reduce nitrate (NO_3^-) > NO_2^- > NO > N_2O > nitrogen gas (N_2), harmless N_2 will be released into the environment where it can eventually become recycled

by nitrogen fixing species (Kuypers et al., 2018). However, it is becoming more clear that the complete reduction of nitrate to nitrogen gas may occur as a polymicrobial community effort in which different members contain only a subset of the denitrification pathway (Gowda et al., 2020; Hester et al., 2019; Lycus et al., 2017; Rich et al., 2003). Synthetic *Pseudomonas aeruginosa* strains have been shown to exchange NO_2^- under strictly anoxic conditions, leading to predictable spatial patterns that are sensitive to pH-dependent abiotic nitrite reduction to toxic nitrogen species (Borer et al., 2020; Lilja and Johnson, 2016). In an independent study, environmental isolates that naturally differed in their possession of denitrification genes were used to create a model that predicted interactions via denitrification intermediates (Gowda et al., 2020); yet, in this case, NO production was only considered for its potential toxicity rather than its potential for energy conservation. Importantly, while older physiological studies have shown that NO can support energy conservation as the sole terminal electron acceptor (Carr et al., 1989; Voβwinkel et al., 1991), to our knowledge, the ability for NO to be exchanged between cells in a manner that supports growth has not be demonstrated.

In this study, we utilized different mutant strains of the denitrifying organism, *P. aeruginosa* strain PA14, to test the hypothesis that the spatial interactions of strains exchanging NO can be predictably altered as a function of oxygen in the microenvironment. *P. aeruginosa* is a cosmopolitan organism, notorious for being an opportunistic human pathogen, but also found in sediments and soils (Arai, 2011). *P. aeruginosa* is also a classic denitrifier that encodes all enzymes necessary for the complete reduction of nitrate to nitrogen gas and can be easily genetically manipulated, permitting the creation of a synthetic NO cross-feeding community. Our findings with this model community provide a conceptual lens through which to interpret more complex microbial community patterning in nature and disease involving the exchange of agathokakological metabolites.

Results

Design and characterization of a synthetic NO cross-feeding community.

The PA14 genome contains a full suite of respiratory enzymes for the complete dissimilatory reduction of NO_3^- to N_2 (Nar, Nap, Nir, Nor, Nos) (Figure 1A) (Arai, 2011), and previous studies have shown that these steps occur sequentially (Carlson and Ingraham, 1983). Accordingly, we hypothesized that it would be possible to partition the PA14 denitrification pathway between two strains, a NO producer and a NO consumer, to make a synthetic community with the ability to catalyze the complete denitrification reaction (Figure 1B, Supplementary file 1A). Several steps were necessary to construct a well-controlled system.

First, we generated a strain of PA14 lacking the nitrate reductase (Δ*narGHJI*, consumer 1, Supplementary file 1A) and grew it in a rich medium anoxically in the presence of nitrate. Compared to wild type PA (WT), growth without nitrate reductase was significantly slower (Supplementary file 1B, orange line). Next, we generated a strain of PA14 lacking the nitric oxide reductase (Δ*norCB*, producer 1; Supplementary file 1A); when grown under the same conditions, this producer strain showed negligible growth (Supplementary file 1C, orange line). This lack of growth was likely due to the reduction of nitrate to NO, which has been measured to build up to 16μM in similar mutants, repressing nitrate reductase expression and preventing further nitrate reduction as a survival mechanism (Yoon et al., 2007). When we mixed these two strains in equal ratios (Supplementary file 1D, orange line), the mixture grew to a higher final OD and nearly twice as fast as the consumer strain.

However, due to the sequential nature of the reduction steps, we realized it was possible that the nitrate reductase mutant (consumer 1) strain could be reducing the NO_2^- intermediate from the nitric oxide reductase mutant (producer 1) strain before NO was even generated (Lilja and Johnson, 2016), or that the producer was benefiting from a secondary crosstalk via N_2O reduction produced by the consumer (Supplementary file 1A, co-culture 1). To eliminate the possibility of these unintended interactions, we removed the nitrite reductase (Nir) from the consumer strain and the nitrous oxide reductase (Nos) from the producer strain (Supplementary file 1A, co-culture 2). Growth of this new producer strain (Δ*norCB*Δ*nosZ*, producer 2) alone was unchanged, indicating that NO growth inhibition or toxicity was still the primary phenotypic driver (Supplementary file 1C, green line). The new consumer strain (Δ*narGHJI*Δ*nirS*, producer 2; Supplementary file 1B, green line) lacking both the nitrate and nitrite reductases, however, showed reduced growth compared to the nitrate-reductase only mutant (Supplementary file 1B, orange line). When these two strains were grown together, there was still a rescue, although slower (Supplementary file 1D, compare orange and green lines). We interpret this difference in growth rate to be due to differential cross-feeding: 1) the strains only cross-feed NO (green trace) or 2) the strains can cross-feed more than NO (yellow trace).

In experiments with our second set of co-culture strains (green), we noticed that the consumer displayed reduced growth upon the removal of nitrite reductase, even though the medium only contained added nitrate. This led us to speculate that the periplasmic nitrate reductase (Nap) might be contributing to consumer growth, or at least reducing the nitrate available to the producer; Nap is commonly thought to be used for redox balancing compared to the membrane bound nitrate reductase (Nar), which contributes to proton translocation and ultimately ATP generation (Richardson, 2000; Sparacino-Watkins et al., 2014; Van Alst et al.,

2009). To test this possibility, we generated a new set of partitioned strains (Supplementary file 1A, co-culture 3, 4), where Nap either was deleted from both the consumer and producer (Δ*narGHJI*Δ*nirS*Δ*napAB*, co-culture 3, purple) or from the consumer only (Δ*norCB*Δ*nosZ*Δ*napAB*, co-culture 4, red). In both cases (Supplementary file 1D) we observed slightly faster growth for the third and fourth co-cultures compared to the second co-culture set, likely due to the restriction of nitrate reduction by the most energetically favorable path (i.e. the producer strain could only reduce nitrate via Nar). Based on these results, for the remainder of our studies, we decided to further investigate the behavior of the nitric oxide producer (Δ*norCB*Δ*nosZ*), consumer (Δ*narGHJI*Δ*nirS*Δ*napAB*), and co-culture described as co-culture 4 (hereafter referred to as the "co-culture") (Figure 1B,C).

To verify that the growth of the strains in the co-culture was due to the removal of NO from the producer by the consumer, in a separate experiment, we functionally replayed the consumer with the chemical NO scavenger, c-PTIO, growing the NO producer strain alone in its presence or absence. In its absence, the producer failed to grow, consistent with the inhibitory effect of NO accumulation. However, the addition of c-PTIO restored growth, supporting the interpretation that NO reduction drives growth in the co-culture (Figure 1D).

Single cell intermixing under planktonic and sessile anoxic conditions suggests NO cross-feeding is mutually beneficial and proximity dependent.

Because our planktonic growth experiments suggested there is a net community benefit to strains in co-culture with a partitioned denitrification pathway under anoxic conditions (Figure 1C), we next sought to determine whether this reflected a mutual or commensal relationship. To address this, we co-cultured and imaged strains expressing constitutive fluorescence markers (GFP or mApple) after 2 days of growth. Population ratios indicated that both strains grew in the co-cultures with the producer having a slight advantage likely due to its ability to continue reducing nitrate (Supplementary file 2A). Swapping the fluorescent proteins between strains did not change this outcome, indicating that this effect is specific to the denitrification effects and not an artefact of GFP or mApple expression. These results suggest that this cross-feeding interaction is mutual (the producer and the consumer represent approximately half of the total population) in which the harm of NO to the producer is alleviated by the consumer, which, in turn, gains an electron acceptor; together, the pathway can proceed.

Building on these results, we wondered how spatial structure might influence the growth of the producer and consumer given that NO is a highly reactive and diffusible molecule. We hypothesized that, unlike under shaken planktonic growth conditions in which the whole

population benefited, under spatially constrained anoxic conditions, proximity would determine the success of community members. To test this prediction, we mixed fluorescently labeled cells of the same or differing genotypes in equal ratios, and then diluted the cultures and sandwiched them between a coverslip and a nitrate-supplemented agar medium pad such that single cells were randomly distributed from one to dozens of cell lengths from each other. From these starting positions, single cells could develop into aggregate biofilms over a 48-hour period. Figure 2A graphically represents the strain mixtures shown in panel B as well as their predicted interactions based on the results of our planktonic growth experiments. As controls, we mixed WT with WT to explore how two cells with the full pathway and no growth defects would interact under these conditions, as well as the consumer and producer strains with themselves. Finally, the producer and consumer strains were mixed to visualize their interaction.

The two strains (GFP/mApple) in the WT mixture grew as large clonal expansions with little single cell intermixing, indicating neither strain was impacted by the other (Ciccarese et al., 2020; Weinstein et al., 2017). In contrast, the consumer mixture showed a dramatic reduction in growth compared to WT, in line with the inability of these strains to reduce nitrate, a terminal electron acceptor. The producer mixture, like the consumer mixture, showed a marked reduction in individual aggregate growth, but also a reduction in total aggregates overall. We infer that the producer strain likely was inhibited for growth but might also have been undergoing lysis. If we compare the WT (Figure 2C) and co-culture (Figure 2D) under these conditions, most strikingly we observe an increase in single cell intermixing between the two strains for the co-culture. The two WT strains (GFP/mApple) appear to grow as clonal expansions, pushing against one another rather than optimizing cell-cell contact. Conversely, the co-culture, although significantly less dense than the WT mixture, appears to favor cell-cell contact between strains and form mixed aggregates, suggestive of a mutual reliance on each other for continued growth. These mixed aggregates were likely the result of close starting positions of producer and consumer cells relative to one another.

In addition to intermixed co-culture aggregates, we also observed a difference in total identifiable aggregates between single genotype mixtures and the co-culture. We observed few producer-only aggregates when grown alone (Supplementary file 2B), likely due to growth inhibition or toxicity of NO. However, when grown in co-culture, we observed an increase in producer aggregate count across several fields of view (Supplementary file 2B). While consumer-only aggregates were initially more numerous than producer-only aggregates (compare Supplementary file 2C “Con” with 2B “Pro”), we found that co-culture with the producer strain increased the variability of consumer aggregate count (Supplementary file 2C).

Importantly, reduction in total aggregates was observed owing to fields of view in which only one intermixed co-culture aggregate was present. These results suggest that while single cell intermixing can occur when the two strains are seeded at close initial starting positions (Figure 2D), NO may also diffuse outward from producer cell aggregates to reach consumer cells at further distances, thereby increasing the interaction range. Together, these results extend our planktonic growth observations into a spatial context, revealing how community members with a partitioned denitrification pathway can interact under anoxic conditions where NO can diffuse.

Oxygen availability induces synthetic community interaction and dials it from a mutualistic (anoxic) to commensal (hyp(oxic)) interaction by increasing NO toxicity.

Recognizing that many environments where denitrification occurs experience variable amounts of oxygen, we wondered what would happen to NO reactivity and in the presence of oxygen. Strains such as PA14 are facultative anaerobes, meaning they preferentially respire oxygen when it is available (oxic conditions), but when oxygen is limited, they induce pathways (such as the denitrification pathway) that permit energy conservation using alternative electron acceptors. A classic example of this phenomenon is when cells grow planktonically but are not shaken during growth. Cells at the surface of the medium reduce oxygen faster than it can diffuse into the medium, resulting in an oxygen gradient (Price-Whelan et al., 2007). To expand our understanding of when, where and how NO-cross feeding operates, we exploited this phenomenon and measured growth in shaking or standing “oxic” cultures. We hypothesized strains harboring a partitioned denitrification pathway would exhibit different behaviors depending on the amount of oxygen and nitrate present, in a manner reflecting the agathokakological effects of oxygen and NO on cells.

To test this hypothesis, we tracked the growth of different producer and consumer strains, alone and in combination, over 48-hours in a continuously shaking plate reader to prevent an oxygen gradient from forming. In the absence of nitrate all strains grew similarly, as expected, indicating the genetic modifications had no off-target effects (Figure 3A). Conversely, when we added 5 mM nitrate to the medium, the consumer strain slightly decreased its growth compared to the WT and the producer strains displayed a brief growth arrest midway through exponential phase, with growth then paralleling that seen for the WT or mixed producer + consumer cultures (Figure 3B). Despite continuous shaking, at these cell densities, we surmise from prior work that these strains began to experience oxygen-limitation during mid exponential phase (Price-Whelan et al., 2007).

To induce hypoxic conditions in a way that oxygen concentration could be measured, we performed the same growth experiment in a plate reader without shaking, thus inducing an oxygen gradient. Again, in the absence of nitrate we did not see a difference between the strains (Figure 3C). However, in the presence of nitrate, growth of the producer and consumer individually slowed compared to the WT but was rescued in co-culture (Figure 3D). Importantly, even without the ability to reduce nitrate, the consumer was able to reach the same final OD as WT, suggesting that while its growth was slowed, it was able to overcome its inability to utilize nitrate as a terminal electron acceptor under these conditions. Conversely, the producer strain(s) showed a dramatic decrease in OD later in the growth curve, suggestive of cell lysis. To validate that an oxygen gradient had formed over time, we used microelectrodes to profile oxgyen concentrations throughout the depth of standing cultures for both WT and the co-culture (Figure 3E).

NO will readily react with superoxide (O_2^-) to form the reactive nitrogen species, peroxynitrite ($ONOO^-$). O_2^- is a by-product and intermediate of oxygen respiration which is removed by superoxide dismutase (SOD), and $ONOO^-$ can out compete superoxide for SOD leading to an accumulation of reactive oxygen species and oxidative stress (Brunelli et al., 1995). Thus, we reasoned that the lysis we observed under hypoxic conditions might be correlated with an increased production of superoxide. To test this idea, we used an intracellular NO sensitive dye (DAF-2DA, Figure 3G) and a superoxide sensitive dye (CellROX, Figure 3F) to detect these metabolites. Both NO and superoxide increased over the growth curve in the producer strain alone (Figure 3F,G), with a rise in signal around 30 hours, correlating with the drop in OD (Figure 3D, arrows, “lysis”).

Differences in the transcriptional regulation of nitrate reductases leads to spatiotemporal control of NO production during aggregate biofilm development.

Based on the observation that the producer’s growth and self-toxicity was correlated with oxygen availability, and because oxygen gradients like those seen in standing cultures (Figure 3E) readily form in biofilm contexts (Arshad et al., 2014; Spero and Newman, 2018; Stewart et al., 2016), we next sought to visualize lysis as a spatial proxy for NO production. To achieve this, we grew diluted cells on agar pads under oxic conditions to form aggregate biofilms, focusing only on NO producing cells. Recalling that the substrate for the nitrite reductase that produces NO can be generated by both Nap and Nar, we compared two different producer strains, one that contained both Nap and Nar and one that only contained Nar (Figure 4A). Because *nap* and *nar* genes are regulated by different transcription factors: *nap* by RpoS

(stationary phase/quorum sensing) (Schuster et al., 2004) and *nar* by ANR (nitrate and low oxygen) (Arai, 2011), we hypothesized that NO production in aggregate biofilm might be a differential spatial distributed as a function of the strain's genomic content and thus transcriptional regulation.

Inoculated agar pads were pre-incubated at 37°C under oxic conditions for 18 hours to enable aggregate biofilm development after which we performed time lapse imaging at 37°C to track subsequent growth and lysis. The producer containing both Nap and Nar grew into overall smaller aggregate biofilms compared to the producer containing Nar only before undergoing a wave of lysis starting at the periphery and moving inward (Figure 4B). High magnification views of lysis illustrate that cells no longer appear black under phase and no longer contain fluorescence (Supplementary file 4A). It is possible that the pattern of lysis observed in the biofilms reflects relatively more NO being made by peripheral cells that have greater access to oxygen and nutrients (Smriga et al., 2021); by the same token, these cells are the first to experience NO-induced toxicity and die. To test this idea, we used the oxidative stress fluorescent probe, CellROX on similar biofilms (containing both Nap and Nar) to visualize local toxicity in relation to cell lysis. Though our planktonic experiments successfully documented a correlation between superoxide and NO production with fluorescent probes (Fig. 3F, 3G), the NO probe was too dim to quantify relative to the autofluorescent background, thus superoxide detection is our proxy for NO. We observed a strong correlation between CellROX intensity patterns and lysis, reinforcing that oxidative stress begins at the periphery and moves towards the center as lysis progresses (Fig. 4D, 4E). Such peripheral death would collapse an oxygen gradient, resulting in a lysis cascade as deeper cells continue to produce NO now in the presence of more oxygen until all cells have lysed.

Conversely, the producer that only contains Nar initially develops into large aggregate biofilms, likely due to little NO production until Nar is activated in response to low oxygen in the interior and the presence of nitrate, leading to internal NO production and lysis (Figure 4C). Interestingly, when we compared CellROX staining of three different producer (Nar) biofilms at different stages of lysis, we also saw a dramatic increase in staining that started centrally and worked its way outward. These results give credence to our model, but also indicate that lysis at the perimeter or core are both due to oxidative stress. This could either be due to trace oxygen being present in the core initially, allowing superoxide production, or anoxic NO buildup inhibiting metabolism, thereby causing a collapse of the oxygen gradient.

Microenvironmental control of NO cross-feeding leads to predictable spatial patterns.

To visualize dynamic interactions between NO producers and consumers, we again mixed the strains with themselves or each other and incubated them under oxic conditions on nutrient agar pads containing nitrate. After 24 hours of growth, we observed that WT, like under anoxic conditions, grew into aggregate biofilms, but rather than as monolayers, these biofilms appeared thicker, perhaps due to the ability to support oxic and anoxic growth (Figure 5A). The consumer mixture also grew into large aggregate biofilms (much larger than under anoxic conditions due to its access to oxygen as a TEA), though the expansions were not as dense due to the inability to support anoxic growth with nitrate (Figure 5A). The producer only mixture again showed lysis (Figure 5A). Strikingly, the border between the the producer and consumer in co-culture was dramatically different.

As seen under anoxic conditions (Figure 2C), WT strains showed no intermixing, suggestive of no interaction/advantage or reliance on each other (Figure 5B). The co-culture, however, showed lysis of producer cells when not in proximity to consumer cells and an increase in single cell intermixing (Figure 5C). This suggests that from the beginning, the co-culture single cells grew into clonal expansions, not interacting until the microenvironment was metabolically altered (depletion of oxygen, beginning utilization of nitrate); the producer began to lyse on its own, but when in proximity to a consumer, was relieved of NO toxicity. In other words, over time, metabolic dynamics unlock a spatial niche where cross-feeding provides a selective advantage. Such protection manifested in several ways (Figure 5D): some producer cells appeared to cling to the consumer cells, following their contour; other producer cells appeared to be protected by a pocket formed by consumer cells; and still others were protected by regions of high intermixing. Knowing that the producer cells would lyse without local NO depletion (Figure 4) permits us to link cellular spatial arrangement to physiological activity. To further test this interpretation, we set up additional pads with the co-culture, pre-incubating them until just before the producer showed lysis, and recording the cellular dynamics over time. As predicted, the producer (Nap/Nar) cells lysed; however, unlike when grown alone where lysis began at the periphery (compare to Figure 4B), the producer in the co-culture experiment showed lysis beginning several cell lengths from the periphery when in close proximity to consumer strains (Figure 5E).

Interestingly, in contrast to mixtures using the Nap/Nar producer (Supplementary file 4A), when the same experiment is performed using the producer that only contains Nar, rescue of the producer is not observed by the consumer, presumably due to NO only being generated in the biofilm core, too far from the consumer to trigger a mutually-beneficial interaction (Supplementary file 4B). These results suggest a model in which initially the two strains do not

interact because they have full access to oxygen and do not yet need nitrate. However, as they grow larger and an oxygen gradient forms in the microenvironment, the producer begins generating NO which leads to self-lysis unless the producer is proximal to the consumer, which relieves the producer's self-toxicity and provides the consumer a terminal electron acceptor (Supplementary file 4C).

Discussion

Microbial metabolism is increasingly appreciated for its contributions to human and environmental health (Hester et al., 2019; Ponomarova and Patil, 2015; Zuñiga et al., 2017), and awareness of the diversity of microbial metabolic interactions is expanding with improved techniques for identifying new pathways and observing interactions (Cordero and Datta, 2016; Dar et al., 2021; DePas et al., 2016; Pessi et al., 2020; Wilbert et al., 2020; Zuñiga et al., 2017). In the face of this progress, gaining a better understanding of how these interactions may shift as a function of dynamic oxygen gradients is an important goal. We developed a synthetic microbial community linked by the exchange of NO, an agathokakological molecule whose biological effects are tuned by the presence of oxygen, as a step towards this end. Our work shows that the interactions that drive NO intercellular exchange and reduction are induced and sensitive to the genetic content of community members and microenvironmental gradients, knowledge of which leads to predictable organizational outcomes.

Differential regulation of the Nar and Nap enzymes, both of which produce nitrite, the metabolic precursor of NO in the denitrification pathway, directly impacts NO producer and consumer interactions. Nar is induced under anoxic conditions and contributes to energy conservation (Arai, 2011) whereas Nap can be expressed in (hyp)oxic environments and facilitates redox balancing (Brondijk et al., 2004; Gates et al., 2008). These differences in regulation thereby control NO production and reduction across a range of oxygen regimes. Linking metabolic interactions to microscale microbial organizations is an important and increasingly appreciated goal (Fuhrman, 2009; Gralka et al., 2020; Kuhns et al., 2015; Ma and Cordero, 2018; Proctor and Relman, 2017; Widder et al., 2016). That genomic content—including regulatory structure—shapes microbial interactions is not surprising, yet the point that differential regulation of key steps in a partitioned metabolic pathway can determine interaction outcomes is important to keep in mind when attempting to understand and predict when and how members of complex microbial communities may spatially associate.

Our findings spotlight local oxygen availability for its ability to tune both the nature and need for a cross-feeding relationship. In our example case, NO can generate toxic byproducts in

the presence of oxygen, leading to cellular growth arrest. Yet in the absence of oxygen, NO can be a lifeline, serving as a terminal electron acceptor and promoting energy conservation and growth. These agathokakological effects are important because oxygen is often heterogeneously available in natural systems, exhibiting steep environmental gradients over small spatial scales (Kolpen et al., 2014; Krichels et al., 2019). Because of this, oxygen availability influences whether strains with a bifurcated denitrification pathway exhibit mutualism (in anoxic environments, growth of the NO producer and consumer is co-dependent) or commensalism (in (hyp)oxic environments, growth of the NO producer is constrained due to toxicity in the absence of the consumer, whereas the consumer does not rely on NO to support growth). Moreover, oxygen gradients can shape microbial interactions both in planktonic and sessile communities, with the scales over which these interactions occur being set by the proximity of interacting cells and their local microenvironment, which they in turn alter in space and time.

While our work with a well-controlled synthetic community allowed us to make these observations, an important next step will be to determine whether mixtures of natural isolates with partitioned metabolic pathways play by the same rules. Our work gives rise to testable predictions about when and where NO cross-feeding may occur. For example, it is well appreciated that NO is an important intermediate species in the nitrogen cycle (Kuypers et al., 2018), whose turnover rates may decide the fate of soil nitrogen stores. Interestingly, recent metagenomic studies indicate that within certain habitats, there an enrichment for organisms that can only reduce NO to N_2O, an important greenhouse gas (Pessi et al., 2020). Thus, an understanding what constrains NO reduction may provide insight into a metabolic process with important environmental consequences. Recent studies have drawn attention to the potential for partitioned pathways to influence the rate of nitrogen flux in soils by resident microbes (Gowda et al., 2020; Pessi et al., 2020). Our work attempts to directly link structure and function of such partitions as is suggested by the genomic content of environmental isolates (Pessi et al., 2020). In an entirely different context, our finding that *P. aeruginosa* can thrive by reducing NO provided by another cell lends credence to the hypothesis that PA may survive the host immune NO attack by its reduction to N_2O, and may correlate with the appearance of N_2O in the breath gas of cystic fibrosis patients (Kolpen et al., 2014). Importantly, *P. aeruginosa* can be found proximal to host immune cells in these infected environments (DePas et al., 2016).

Finally, we note that NO is only one of many agathokakological molecules, both organic and inorganic, that may help structure microbial communities over small spatial scales as a function of oxygen availability. For example, other redox-active metabolites such as phenazines

441 can function as natural toxins or beneficial agents of nutrient acquisition and/or redox
442 homeostasis, depending on the microenvironmental context (Dahlstrom et al., 2020). Similarly,
443 sulfide has long been known to play nuanced roles in nature, with its concentration-dependent
444 toxicity influencing which phototrophic species are able to thrive (Findlay et al., 2015), and
445 where different energy-conserving processes can occur within microbial mats (Jungblut et al.,
446 2016; Prieto-Barajas et al., 2018). We hasten to note that many other parameters may be
447 subject to similar dynamic spatiotemporal gradients, such as carbon, pH and light, and are likely
448 to also play important roles in determining the niches where cross-feeding or other types of
449 metabolic interactions can occur (Zhang et al., 2021). Towards the goal of gaining a predictive
450 understanding of why diverse microbial communities are structured the way they are, a
451 constructive next step will be to model these interactions, iterating with experiments until cross-
452 cutting principles can be identified with predictive power.
453
454 **Materials and methods**
455 **Bacterial strains and growth conditions.** All strains used are clean deletion mutants
456 originating from the wild-type (WT) *Pseudomonas aeruginosa* UCBPP-PA14 strain as described
457 below. Strains were stored as 50% glycerol stocks at -80°C. Before use, strains were streaked
458 from frozen stock onto Bacto agar (BD, Sigma) plates containing LB (Miller, BD, Sigma) or LB
459 supplemented with 50ug/mL gentamicin (GoldBio) to select for retention of expression cassettes
460 within fluorescent strains, and grown overnight at 37°C. From streak plates, a dab of culture was
461 used to inoculate 5mL liquid cultures in LB or LB plus 50ug/mL gentamicin liquid media.
462 Cultures were shaken at 250rpm at 37°C overnight until fully saturated at stationary phase. To
463 standardize inoculum sizes between strains, each strain's optical density (OD_{500nm}) was
464 measured by spectrophotometry (Beckman Coulter). Strains were then each washed and
465 diluted to an OD of 1 via centrifugation and resuspension in 1X phosphate buffered saline
466 (PBS). Strains were then either further diluted directly, or first mixed at equal ratios for co-
467 culture experiments. For all experiments, we used a Low Salt LB (LSLB) in place of standard LB
468 powder due to microelectrode reactivity to high NaCl in LB. The composition of LSLB is 141mM
469 Tryptone (BD, Sigma), 16mM Yeast Extract (BD, Sigma), 45mM NaCl (Fisher Chemical), which
470 were dissolved in Mili-Q water and autoclaved. 5mM Nitrate was supplemented into LB or LSBL
471 where indicated by diluting from a 1M stock of KNO_3 (Fisher Chemical).
472
473 **Construction of mutant bacterial strains.** Table S1 contains a full list of primers used in the
474 creation of deletion constructs and mutant strains used in this study. Briefly, a 1kb fragment up-

and downstream of the target gene was amplified via PCR and cloned into the pMQ30 plasmid using Gibson cloning (NEB) and transformed into *E. coli* cells as previously described (Spero and Newman, 2018). Deletion constructs were then introduced to parent strains (WT PA14 and or deletion strains of PA14, see Table S1) via triparental conjugation. *E. coli* plasmid and helper strains were selected against by bead plating conjugation onto VBMM plates containing 50ug/mL gentamicin (Choi and Schweizer, 2006). Clean deletion strains were then bead plated on a 10% sucrose plate to induce homologous recombination with the construct containing the regions up- and downstream, but lacking the targeted gene locus (Basta et al., 2017). Mutant strains were confirmed first by patching on sucrose and gentamicin plates, and successful mutants grew on sucrose but not gentamicin. Next, PCR genotyping was performed using primers that span the deletion region, sequencing confirmed the identity of these deletions, and anaerobic growth challenges revealed expected physiological effects (e.g. ΔnirS was unable to grow on nitrite, etc). Fluorescence strains were created as previously describe (Basta et al., 2017; Meirelles and Newman, 2018) using fluorescent GFP/mApple plasmids driven by the constative ribosomal promoter rpsG introduced into the Tn7 site of specified strains using tetra-parental conjugation. *E. coli* helper strains were again selected against using VBMM containing 50ug/mL gentamicin. Confirmation of insertion was performed via microscopy, visualizing colonies in both green and red fluorescence channels and selecting those that were bright in their respective channel. Frozen stocks were also used to start cultures and image single cells which showed significant fluorescence in appropriate channels above background autofluorescence.

Growth curves. Anoxic growth curve media was placed in anaerobic chamber 72 hours prior to experiment to allow time for oxygen to degas from media. 1 OD_{500nm} cultures were brought into chamber and further diluted to 0.005 OD_{500nm} in anoxic media. Growth curves were performed using a BioTek Synergy 4 plate reader stored in an anoxic chamber and set to 37C with shaking and measured OD_{500nm} every 10 minutes. Oxic (shaking) and Hypoxic (stationary) growth curves were set up as above but under normal atmosphere. Oxic growth curves were performed using a Tecan Spark 10M set to orbital shaking. Hypoxic growth curves were performed using a Spectramax M3 (Molecular Devices) plate reader set to not shake. Each condition was performed in technical triplicate or quadruplicate. Each well contained 200 µl of culture with 40uL of mineral oil added to the top of each well to prevent evaporation of 48-72-hour growth curves. Traces from all growth curves (Figure 1, Figure 3, Supplementary file 1) were analyzed

by plotting mean OD_{500nm} over time (dark center line) as well as 95% confidence intervals from the technical replicates (shaded area) using Seaborn plotting packages in Python.

Nitric oxide and superoxide quantification. Levels of nitric oxide and superoxide were quantitated using fluorescent dyes during hypoxic growth curves. NO was quantitated using 50μM DAF-2DA (Calbiochem, Sigma) which is internalized by cells where esterases free DAF-2DA to interact with NO producing a green fluorescence signal (Aakanksha Wany, Pradeep Kumar Pathak, 2020). Superoxide was quantitated using 5μM CellROX Deep Red (Thermo), which is non-fluorescent in a reduced state but exhibits a strong induction of fluorescence upon oxidation with reactive oxygen species (McBee et al., 2017). To measure these probes, a hypoxic growth curve in LSLB with or without 5mM KNO_3 was performed as indicated above and the Spectramax plate reader was configured to additionally measure green fluorescence (Ex. 488nm, Em. 520nm, DAF-2) and far red fluorescence (Ex. 640nm, Em. 665nm, CellROX). For pad imaging assays, CellROX was supplemented to the agar pads directly at a final concentration of 10μM and imaged after significant biofilm growth had occurred to reveal superoxide localization. DAF-2DA was also used to visualize NO, however, due to weak single-cell signal and strong background autofluorescence in the green channel, we were unable to visualize the signal.

Oxygen profiling. To confirm the presence of oxygen gradients in standing cultures, we employed a 25μm diameter oxygen microelectrode electrode (Unisense), which was calibrated as previously described (Spero and Newman, 2018). Briefly, LSLB media incubated at 37°C was used to calculate the high point O_2 concentration. A zero-point calibration was obtained by dissolving 2g Sodium Ascorbate in 100mL 0.1 NaOH, which scavenges O_2 from the medium. Using the Unisense Sensor Suite Software to save calibration values and to control a motorized micromanipulator to perform profiling, O_2 was measured from the surface of hypoxically incubated planktonic cultures in 1mL Eppendorf tubes. The surface was set by eye and confirmed by a reduction in mV signal. O_2 was then measured over a 1mm distance below the surface at 50μm intervals. Two measurements were taken at each position, and three technical replicates were averaged and displayed as the mean value with 95% confidence intervals (Figure 3E). Cultures were prepared as in growth curves but maintained as 1mL volumes in tubes rather than aliquoting into 96-well plates. Mineral oil was not added due to potential incompatibility with electrodes.

Agar pad imaging assay. After significant optimization, it was determined that 1 OD_{500nm} cultures diluted to a starting concentration of 0.001 OD_{500nm} was sufficient to obtain single cells randomly distributed under agar pads. Agar pads were made by combining LSLB media with or without 5mM KNO_3, with 2% w/v Noble Agar (BD, Sigma). Prior to use, the agar was melted by microwaving. To make equally sized agar pads, 100µL was pipetted into each of several square molds (6-7mm X 7mm X 1.6mm Depth ID, 25mm X 75mm, Grace Bio Labs), placed between two glass microscope slides, and allowed to solidify at 4°C until use. Anoxic pads were made 72 hours in advance and placed in an anaerobic chamber to degas. 5 µL of 0.001 OD_{500nm} dilution culture was added to the bottom of a well in an 8-well LabTek dish (Thermo). An agar pad was then placed on top of the culture. LabTek cultures were incubated at 37°C for 24 hours (oxic) or 48 hours (anoxic) in a sealed container (6.7ounce, Systema). Importantly, when additional humidity was added using a wet tissue under samples, instead of distinct aggregate biofilms, cells grew more like intermixed planktonic cultures; thus, additional humidity was not added. Time lapse imaging of pads was performed by first incubating pads as described above, but just before lysis would occur (empirically determined to be at approximately 18 hours), LabTek cultures were sealed with parafilm to prevent evaporation in the heated microscope incubation chamber. Anoxically-incubated cells were not initially fluorescent upon removal from chamber to image due to an inability for fluorophores to fold in the absence of oxygen. To overcome this, pads were placed at 4ºC without lids for one to two hours prior to imaging which resulted in sufficient signal recovering to differentiate between GFP and mApple cells.

Imaging and image analyses. All imaging was performed using a Nikon Ti2 widefield fluorescence microscope. End time point images were collected using a Plan Fluor 100x/1.30 oil phase objective and time lapse images were collected using a Plan Apo 40x/0.90 dry phase objective. GFP channel used a 488nm LED excitation light source and emission was collected with a FITC filter. The mApple channel used 561nm LED light source and emission was collected with a TRITC filter. For time lapse imaging, an OKO Labs cage incubation unit was set to 37°C several hours before imaging to equilibrate the microscope stand and used for the duration of the imaging experiment. Images were collected every 20 minutes from multiple stage positions. Time indicated in figures (Figure 4B,C, Figure 5E) represents time since the pads were inoculated. Images were analyzed and prepared for display using FIJI (Schindelin et al., 2012). Anoxically-incubated cells showed significantly less fluorescence than oxically incubated ones; in order to optimally observe cells over background, a background subtraction using FIJI's built-in function was performed. Brightness and contrast were adjusted on a per image basis in

order to best display cell positions and identifications, unless otherwise noted (e.g. CellROX intensity in biofilms imaged and displayed the same for comparison of intensity (Figure 4D)). To account for significant drift of the agar pads during time lapse imaging and produce the videos and montages displayed herein, an image registration was performed using the StackReg plugin with the Rigid Body choice. Image segmentation was used to quantify the ratio of GFP:mApple cells in the anoxic planktonic cultures (Supplementary file 2A),. Briefly, contrast was enhanced, background subtracted fluorescence channels were combined to create a total cell mask. The Auto local Threshold function with the Phansalkar selection was used to segment and count both the total and GFP channel cells. Because cells appeared to become more fluorescent in the mApple channel during long anoxic incubations, this prevented us from being able to segment mApple cells directly. Therefore, we calculated mApple cell counts as total cell counts minus GFP cell counts, then used these values to compute population percentages.

Acknowledgments. The work was supported by the National Institutes of Health (R01HL152190 to D.K.N.) and the National Science Foundation Graduate Student Fellowships Program (to S.A.W.). We would like to thank the current and past Newman Lab members for feedback and discussions. Specifically, we thank Drs. Darcy McRose and Avi Flamholz for critical manuscript review, Dr. Melanie Spero for molecular technique instruction, Drs. Reinaldo Alcade and Georgia Squyres for fruitful discussion and troubleshooting imaging assays, and Dr. Michael Piacentino for help with coding and general morale.

Competing interests. The authors declare no conflict of interests.

References

Aakanksha Wany, Pradeep Kumar Pathak and KJG. 2020. Methods for Measuring Nitrate Reductase, Nitrite Levels, and Nitric Oxide from Plant Tissues Aakanksha **2057**:5–6.

Arai H. 2011. Regulation and Function of Versatile Aerobic and Anaerobic Respiratory Metabolism in Pseudomonas aeruginosa. *Front Microbiol* **2**:103. doi:10.3389/fmicb.2011.00103

Arshad TA, Bonnecaze RT, Shear JB, Whiteley M, Wessel AK, Connell JL, Fitzpatrick M. 2014. Oxygen Limitation within a Bacterial Aggregate. *MBio* **5**. doi:10.1128/mbio.00992-14

Basta DW, Bergkessel M, Newman DK. 2017. Identification of fitness determinants during energy-limited growth arrest in Pseudomonas aeruginosa. *MBio* **8**:1–17. doi:10.1128/mBio.01170-17

Borer B, Ciccarese D, Johnson D, Ori D. 2020. Spatial organization in microbial range expansion emerges from trophic dependencies and successful lineages Benedict. *Commun Biol* 1–10. doi:10.1038/s42003-020-01409-y

Brondijk THC, Nilavongse A, Filenko N, Richardson DJ, Cole JA. 2004. NapGH components of the periplasmic nitrate reductase of Escherichia coli K-12: Location, topology and physiological roles in quinol oxidation and redox balancing. *Biochem J* **379**:47–55. doi:10.1042/BJ20031115

Brunelli L, Crow JP, Beckman JS. 1995. The comparative toxicity of nitric oxide and peroxynitrite to escherichia coli. *Arch Biochem Biophys*. doi:10.1006/abbi.1995.1044

Carlson CA, Ingraham JL. 1983. Comparison of denitrification by Pseudomonas stutzeri, Pseudomonas aeruginosa, and paracoccus denitrificans. *Appl Environ Microbiol* **45**:1247–1253. doi:10.1128/aem.45.4.1247-1253.1983

Carr GJ, Page MD, Ferguson SJ. 1989. The energy-conserving nitric-oxide-reductase system in Paracoccus denitrificans Distinction from the nitrite reductase that catalyses synthesis of nitric oxide and evidence from trapping experiments for nitric oxide as a free intermediate during denitrifi. *Eur J Biochem* **179**:683–692. doi:10.1111/j.1432-1033.1989.tb14601.x

Choi KH, Schweizer HP. 2006. mini-Tn7 insertion in bacteria with single attTn7 sites: Example Pseudomonas aeruginosa. *Nat Protoc* **1**:153–161. doi:10.1038/nprot.2006.24

Ciccarese D, Zuidema A, Merlo V, Johnson DR. 2020. Interaction-dependent effects of surface structure on microbial spatial self-organization. *Philos Trans R Soc B Biol Sci* **375**:20190246. doi:10.1098/rstb.2019.0246

Cordero OX, Datta MS. 2016. Microbial interactions and community assembly at microscales. *Curr Opin Microbiol* **31**:227–234. doi:10.1016/j.mib.2016.03.015

634 Dahlstrom KM, McRose DL, Newman DK. 2020. Keystone metabolites of crop rhizosphere
635 microbiomes. *Curr Biol* **30**:R1131–R1137. doi:10.1016/j.cub.2020.08.005
636 Dal Co A, Ackermann M, van Vliet S. 2019. Metabolic activity affects response of single cells to
637 a nutrient switch in structured populations. *bioRxiv*. doi:10.1101/580563
638 Dar D, Dar N, Cai L, Newman DK. 2021. In situ single-cell activities of microbial populations
639 revealed by spatial transcriptomics. *bioRxiv* 2021.02.24.432792.
640 DePas WH, Starwalt-Lee R, Van Sambeek L, Kumar SR, Gradinaru V, Newman DK. 2016.
641 Exposing the three-dimensional biogeography and metabolic states of pathogens in cystic
642 fibrosis sputum via hydrogel embedding, clearing, and rRNA labeling. *MBio* **7**:1–11.
643 doi:10.1128/mBio.00796-16
644 Fang Y, Koba K, Makabe A, Takahashi C, Zhu W, Hayashi T, Hokari AA, Urakawa R, Bai E,
645 Houlton BZ, Xi D, Zhang S, Matsushita K, Tu Y, Liu D, Zhu F, Wang Z, Zhou G, Chen D,
646 Makita T, Toda H, Liu X, Chen Q, Zhang D, Li Y, Yoh M. 2015. Microbial denitrification
647 dominates nitrate losses from forest ecosystems. *Proc Natl Acad Sci U S A* **112**:1470–
648 1474. doi:10.1073/pnas.1416776112
649 Findlay AJ, Bennett AJ, Hanson TE, Luther GW. 2015. Light-dependent sulfide oxidation in the
650 anoxic zone of the chesapeake bay can be explained by small populations of phototrophic
651 bacteria. *Appl Environ Microbiol* **81**:7560–7569. doi:10.1128/AEM.02062-15
652 Fuhrman JA. 2009. Microbial community structure and its functional implications. *Nature*
653 **459**:193–199. doi:10.1038/nature08058
654 Gates AJ, Richardson DJ, Butt JN. 2008. Voltammetric characterization of the aerobic energy-
655 dissipating nitrate reductase of Paracoccus pantotrophus: Exploring the activity of a redox-
656 balancing enzyme as a function of electrochemical potential. *Biochem J* **409**:159–168.
657 doi:10.1042/BJ20071088
658 Goldford JE, Lu N, Bajić D, Estrela S, Tikhonov M, Sanchez-Gorostiaga A, Segrè D, Mehta P,
659 Sanchez A. 2018. Emergent simplicity in microbial community assembly. *Science (80-)*
660 **361**:469–474. doi:10.1126/science.aat1168
661 Gowda K, Ping D, Mani M, Kuehn S. 2020. A sparse mapping of structure to function in
662 microbial communities. *bioRxiv* 1–16.
663 Gralka M, Szabo R, Stocker R, Cordero OX. 2020. Trophic Interactions and the Drivers of
664 Microbial Community Assembly. *Curr Biol* **30**:R1176–R1188.
665 doi:10.1016/j.cub.2020.08.007
666 Hester ER, Jetten MSM, Welte CU, Lücker S. 2019. Metabolic overlap in environmentally
667 diverse microbial communities. *Front Genet* **10**:1–10. doi:10.3389/fgene.2019.00989

668 Jungblut AD, Hawes I, Mackey TJ, Krusor M, Doran PT, Sumner DY, Eisen JA, Hillman C,
669 Goroncy AK. 2016. Microbial mat communities along an oxygen gradient in a perennially
670 ice-covered Antarctic lake. *Appl Environ Microbiol* **82**:620–630. doi:10.1128/AEM.02699-15
671 Kalkowski I. 1991. Metabolism of nitric oxide in denitrifying Pseudomonas aeruginosa and
672 nitrate-respiring Bacillus cereus. *FEMS Microbiol Lett* **82**:107–112. doi:10.1016/0378-
673 1097(91)90429-E
674 Kolpen M, Kühl M, Bjarnsholt T, Moser C, Hansen CR, Liengaard L, Kharazmi A, Pressler T,
675 Høiby N, Jensen PØ. 2014. Nitrous oxide production in sputum from cystic fibrosis patients
676 with chronic Pseudomonas aeruginosa lung infection. *PLoS One* **9**.
677 doi:10.1371/journal.pone.0084353
678 Koppenol H, Koppenol H. 2021. Nitric oxide, superoxide, and peroxynitrite: the good, the bad,
679 and the ugly.
680 Koskenkorva T, Aro-Kärkkäinen N, Bachmann D, Arai H, Frey AD, Kallio PT. 2008.
681 Transcriptional activity of Pseudomonas aeruginosa fhp promoter is dependent on two
682 regulators in addition to FhpR. *Arch Microbiol* **189**:385–396. doi:10.1007/s00203-007-0329-
683 3
684 Krichels A, DeLucia EH, Sanford R, Chee-Sanford J, Yang WH. 2019. Historical soil drainage
685 mediates the response of soil greenhouse gas emissions to intense precipitation events.
686 *Biogeochemistry* **142**:425–442. doi:10.1007/s10533-019-00544-x
687 Krichels AH, Yang WH. 2019. Dynamic Controls on Field-Scale Soil Nitrous Oxide Hot Spots
688 and Hot Moments Across a Microtopographic Gradient. *J Geophys Res Biogeosciences*
689 **124**:3618–3634. doi:10.1029/2019JG005224
690 Kuhns DB, Priel DAL, Chu J, Zarember KA. 2015. Isolation and Functional Analysis of Human
691 Neutrophils. *Curr Protoc Immunol* **111**:139–148. doi:10.1002/0471142735.im0723s111
692 Kuypers MMM, Marchant HK, Kartal B. 2018. The microbial nitrogen-cycling network. *Nat Rev*
693 *Microbiol* **16**:263–276. doi:10.1038/nrmicro.2018.9
694 Lilja EE, Johnson DR. 2016. Segregating metabolic processes into different microbial cells
695 accelerates the consumption of inhibitory substrates. *ISME J* **10**:1568–1578.
696 doi:10.1038/ismej.2015.243
697 Lowery NV, Ursell T. 2019. Structured environments fundamentally alter dynamics and stability
698 of ecological communities. *Proc Natl Acad Sci U S A* **116**:379–388.
699 doi:10.1073/pnas.1811887116
700 Lycus P, Bøthun KL, Bergaust L, Shapleigh JP, Bakken LR, Frostegård Å. 2017. Phenotypic
701 and genotypic richness of denitrifiers revealed by a novel isolation strategy. *ISME J*

11:2219–2232. doi:10.1038/ismej.2017.82

Ma L, Cordero OX. 2018. Solving the structure-function puzzle. *Nat Microbiol* **3**:750–751. doi:10.1038/s41564-018-0186-7

Meirelles LA, Newman DK. 2018. Both toxic and beneficial effects of pyocyanin contribute to the lifecycle of Pseudomonas aeruginosa. *Mol Microbiol* **110**:995–1010. doi:10.1111/mmi.14132

Niehaus L, Boland I, Liu M, Chen K, Fu D, Henckel C, Chaung K, Miranda SE, Dyckman S, Crum M, Dedrick S, Shou W, Momeni B. 2019. Microbial coexistence through chemical-mediated interactions. *Nat Commun* **10**. doi:10.1038/s41467-019-10062-x

Pessi IS, Viitamäki S, Eronen-Rasimus E, Delmont TO, Luoto M, Hultman J. 2020. Truncated denitrifiers dominate the denitrification pathway in tundra soil metagenomes. *bioRxiv*. doi:10.1101/2020.12.21.419267

Ponomarova O, Patil KR. 2015. Metabolic interactions in microbial communities: Untangling the Gordian knot. *Curr Opin Microbiol* **27**:37–44. doi:10.1016/j.mib.2015.06.014

Price-Whelan A, Dietrich LEP, Newman DK. 2007. Pyocyanin alters redox homeostasis and carbon flux through central metabolic pathways in Pseudomonas aeruginosa PA14. *J Bacteriol* **189**:6372–6381. doi:10.1128/JB.00505-07

Prieto-Barajas CM, Valencia-Cantero E, Santoyo G. 2018. Microbial mat ecosystems: Structure types, functional diversity, and biotechnological application. *Electron J Biotechnol* **31**:48–56. doi:10.1016/j.ejbt.2017.11.001

Proctor DM, Relman DA. 2017. The Landscape Ecology and Microbiota of the Human Nose, Mouth, and Throat. *Cell Host Microbe*. doi:10.1016/j.chom.2017.03.011

Ratzke C, Barrere J, Gore J. 2020. Strength of species interactions determines biodiversity and stability in microbial communities. *Nat Ecol Evol* **4**:376–383. doi:10.1038/s41559-020-1099-4

Rich JJ, Heichen RS, Bottomley PJ, Cromack K, Myrold DD. 2003. Community Composition and Functioning of Denitrifying Bacteria from Adjacent Meadow and Forest Soils. *Appl Environ Microbiol* **69**:5974–5982. doi:10.1128/AEM.69.10.5974-5982.2003

Richardson DJ. 2000. Bacterial respiration: a flexible process for a changing environment. *Microbiology* **146 (Pt 3**:551–571. doi:10.1099/00221287-146-3-551

Sasaki Y, Oguchi H, Kobayashi T, Kusama S, Sugiura R, Moriya K, Hirata T, Yukioka Y, Takaya N, Yajima S, Ito S, Okada K, Ohsawa K, Ikeda H, Takano H, Ueda K, Shoun H. 2016. Nitrogen oxide cycle regulates nitric oxide levels and bacterial cell signaling. *Sci Rep* **6**:1–11. doi:10.1038/srep22038

736 Schindelin J, Arganda-Carreras I, Frise E, Kaynig V, Longair M, Pietzsch T, Preibisch S,
737 Rueden C, Saalfeld S, Schmid B, Tinevez JY, White DJ, Hartenstein V, Eliceiri K,
738 Tomancak P, Cardona A. 2012. Fiji: An open-source platform for biological-image analysis.
739 *Nat Methods* **9**:676–682. doi:10.1038/nmeth.2019
740 Schuster M, Hawkins AC, Harwood CS, Greenberg EP. 2004. The Pseudomonas aeruginosa
741 RpoS regulon and its relationship to quorum sensing. *Mol Microbiol* **51**:973–985.
742 doi:10.1046/j.1365-2958.2003.03886.x
743 Smriga S, Ciccarese D, Babbin AR. 2021. Denitrifying bacteria respond to and shape
744 microscale gradients within particulate matrices. *Commun Biol* **4**:570. doi:10.1038/s42003-
745 021-02102-4
746 Sparacino-Watkins C, Stolz JF, Basu P. 2014. Nitrate and periplasmic nitrate reductases.
747 AUTHOR'S MANUSCRIPT. *Chem Soc Rev* **43**:676–706. doi:10.1039/c3cs60249d.Nitrate
748 Spero MA, Newman DK. 2018. Chlorate Specifically Targets Oxidant-Starved, Antibiotic-
749 Tolerant Populations of Pseudomonas aeruginosa Biofilms Melanie. *MBio* **9**:e01400-18.
750 Stewart PS, Zhang T, Xu R, Pitts B, Walters MC, Roe F, Kikhney J, Moter A. 2016. Reaction-
751 diffusion theory explains hypoxia and heterogeneous growth within microbial biofilms
752 associated with chronic infections. *npj Biofilms Microbiomes* **2**:1–8.
753 doi:10.1038/npjbiofilms.2016.12
754 Tian H, Yang J, Xu R, Lu C, Canadell JG, Davidson EA, Jackson RB, Arneth A, Chang J, Ciais
755 P, Gerber S, Ito A, Joos F, Lienert S, Messina P, Olin S, Pan S, Peng C, Saikawa E,
756 Thompson RL, Vuichard N, Winiwarter W, Zaehle S, Zhang B. 2019. Global soil nitrous
757 oxide emissions since the preindustrial era estimated by an ensemble of terrestrial
758 biosphere models: Magnitude, attribution, and uncertainty. *Glob Chang Biol* **25**:640–659.
759 doi:10.1111/gcb.14514
760 Van Alst NE, Sherrill LA, Iglewski BH, Haidaris CG. 2009. Compensatory periplasmic nitrate
761 reductase activity supports anaerobic growth of Pseudomonas aeruginosa PAO1 in the
762 absence of membrane nitrate reductase. *Can J Microbiol* **55**:1133–1144. doi:10.1139/W09-
763 065
764 VoBwinkel R, Neidt I, Bothe H. 1991. The production and utilization of nitric oxide by a new,
765 denitrifying strain of Pseudomonas aeruginosa. *Arch Microbiol* **156**:62–69.
766 doi:10.1007/BF00418189
767 Volk N., Vollmer D, Schmidt M, Oppermann W, Huber K. 2004. Nitric Oxide, an Old Molecule
768 With Noble Functions in Pseudomonas aeruginosa Biology. *Adv Polym Sci* **166**:29–65.
769 doi:10.1016/j.cossms.2010.07.001

Weinstein BT, Lavrentovich MO, Möbius W, Murray AW, Nelson DR. 2017. Genetic drift and selection in many-allele range expansions, bioRxiv. doi:10.1101/145631

Widder S, Allen RJ, Pfeiffer T, Curtis TP, Wiuf C, Sloan WT, Cordero OX, Brown SP, Momeni B, Shou W, Kettle H, Flint HJ, Haas AF, Laroche B, Kreft JU, Rainey PB, Freilich S, Schuster S, Milferstedt K, Van Der Meer JR, Grobkopf T, Huisman J, Free A, Picioreanu C, Quince C, Klapper I, Labarthe S, Smets BF, Wang H, Soyer OS, Allison SD, Chong J, Lagomarsino MC, Croze OA, Hamelin J, Harmand J, Hoyle R, Hwa TT, Jin Q, Johnson DR, de Lorenzo V, Mobilia M, Murphy B, Peaudecerf F, Prosser JI, Quinn RA, Ralser M, Smith AG, Steyer JP, Swainston N, Tarnita CE, Trably E, Warren PB, Wilmes P. 2016. Challenges in microbial ecology: Building predictive understanding of community function and dynamics. *ISME J* **10**:2557–2568. doi:10.1038/ismej.2016.45

Wilbert SA, Mark Welch JL, Borisy GG. 2020. Spatial Ecology of the Human Tongue Dorsum Microbiome. *Cell Rep* **30**:4003-4015.e3. doi:10.1016/j.celrep.2020.02.097

Yoon SS, Karabulut AC, Lipscomb JD, Hennigan RF, Lymar S V., Groce SL, Herr AB, Howell ML, Kiley PJ, Schurr MJ, Gaston B, Choi KH, Schweizer HP, Hassett DJ. 2007. Two-pronged survival strategy for the major cystic fibrosis pathogen, Pseudomonas aeruginosa, lacking the capacity to degrade nitric oxide during anaerobic respiration. *EMBO J* **26**:3662–3672. doi:10.1038/sj.emboj.7601787

Yu K, Mitchell C, Xing Y, Magliozzo RS, Bloom BR, Chan J. 1999. Toxicity of nitrogen oxides and related oxidants on mycobacteria: M. tuberculosis is resistant to peroxynitrite anion. *Tuber Lung Dis* **79**:191–198. doi:10.1054/tuld.1998.0203

Zhang IH, Mullen S, Ciccarese D, Dumit D, Martocello DE, Toyofuku M, Nomura N, Smriga S, Babbin AR. 2021. Ratio of organic carbon to fixed nitrogen regulates metabolic specialization and denitrification dynamics in Pseudomonas aeruginosa. Front Microbiol 12:1-13. https://doi.org/10.3389/fmicb.2021.711073

Zumft WG. 1997. Cell biology and molecular basis of denitrification. *Microbiol Mol Biol Rev* **61**:533–616. doi:10.1128/mmbr.61.4.533-616.1997

Zuñiga C, Zaramela L, Zengler K. 2017. Elucidation of complexity and prediction of interactions in microbial communities. *Microb Biotechnol* **10**:1500–1522. doi:10.1111/1751-7915.12855

Figure Legends

Figure 1. Design and characterization of synthetic nitric oxide cross-feeding community. (**A**) WT PA14 denitrification pathway (**B**) Schematic of NO consumer and producer strains where genes that have been deleted are grayed-out, and those remaining are shown in black. The pathway partitions where NO is produced and reduced. (**C**) Growth curve of co-culture 4 members grown individually and together, compared to the WT, over 72hrs under anoxic conditions with nitrate provided as sole terminal electron acceptor (TEA). (**D**) Growth rescue of producer strain using the chemical NO scavenger c-PTIO.

Supplemental file 1. Synthetic NO cross-feeding co-culture comparisons. (**A**) Schematic representation of genomic identity of consumer and producer strains as done Figure 1B. Wiggly arrows indicate intermediates that can be exchanged. (**B**) Growth curves for specified strains/co-cultures.

Figure 2. Patterning of producer and consumer strains under sessile anoxic conditions. (**A**) Phenotypic predictions. (**B**) Representative images showing growth patterns of indicated strain mixtures constitutively expressing either GFP or mApple after anoxic growth for 48hrs under an agar pad with nitrate provided as sole TEA. (**C,D**) Zoom-in of WT mixture showing strains growing as clonal patches (C) compared with zoom-in of the co-culture showing intermixing (**D**). Consumer strain is Δ*narGHJI*Δ*nirS*Δ*napAB*. Producer strain is Δ*norCB*Δ*nosZ*.

Supplementary file 2. Planktonic culture population ratios and sessile aggregate counts. (**A**) Co-culture 4 and 3 were grown as specified for the anoxic growth curves (Figure 1) but with fluorescence constructs to identify the compositional ratio. Co-cultures with the consumer expressing GFP and producer expressing mApple (left two datasets) were compared to the reciprocal cultures with consumer expressing mApple and producer expressing GFP (right two datasets). (**B**) Producer aggregates when grown alone (Pro.) vs. in co-culture with the consumer (Pro. + Con.). (**C**) Consumer aggregates when grown alone (Con.) vs in co-culture with the producer (Con. + Pro.). Consumer strain is Δ*narGHJI*Δ*nirS*Δ*napAB*. Producer strain is Δ*norCB*Δ*nosZ*.

Figure 3. Oxic vs hypoxic growth of planktonic cultures supplemented with and without nitrate. (**A-D**) 48hr growth curves cultured under the indicated conditions. Evenly oxygenated environments (“oxic-

837 shaking") were achieved by shaking cultures during incubation (A,B), while unevenly oxygenated
838 environments ("hypoxic-stagnant") were achieved by culturing without shaking (C,D). (**E**) Oxygen
839 profiles from non-shaking cultures of the WT compared to profiles from the co-culture at two time
840 points. (**F,G**) Fluorescent dye readings of superoxide and nitric oxide accumulation over a hypoxic
841 growth curve with nitrate (as in D).
842
843 **Figure 4.** Spatiotemporal patterning of lysis within aggregate biofilms as a function of which nitrate
844 reductase is present. **A**) Transcriptional regulatory control of Nap/Nar gene expression (left).
845 Predictions of spatial Nap and Nar activity in a biofilm, given this regulation (right). Nap can reduce
846 nitrate (NO_3^-) to nitrite (NO_2^-) throughout biofilm, and reduction at the surface prevents nitrate diffusion
847 into the biofilm core. Without Nap, nitrate may penetrate deeper. (**B**) Time lapse of producer (Nap/Nar)
848 biofilm lysis occurring from the periphery inward. (**C**) Time lapse of producer (Nar) biofilm lysis
849 occurring from the core outward. (**D**) At the same time point, three distinct representative biofilms
850 arranged by amount of lysis observed per producer type. Red channel represents CellROX staining
851 indicating presence of superoxide. All images are displayed using the same display settings for direct
852 comparison. (**E**) Schematic interpretation of results. NO leads to superoxide production; superoxide
853 localization correlates with lysis: left represents the dynamic for a Nap/Nar producer, right represents
854 the dynamic for a Nar producer.
855
856 **Supplementary file 3.** Visualization of lysis in a Nap/Nar producer biofilm. High magnification image
857 showing lysis, which is interpreted from a loss of fluorescence and increase in transparency in phase
858 contrast.
859
860 **Figure 5.** Patterning of producer and consumer strains under sessile oxic conditions. (**A**)
861 Representative images of indicated strains grown as biofilms for 24hrs under oxic conditions in the
862 presence of nitrate. (**B**) Zoom-in of WT clonal expansion showing no intermixing. (**C**) Zoom-in of co-
863 culture 4 showing producer survival adjacent to the consumer expansion interface; note that cells
864 appear brightest prior to lysis. (**D**) Three additional high magnification callouts to spotlight specific
865 structural features. (**E**) Time lapse of co-culture 4 showing temporal producer lysis occurring in the
866 absence of consumer contact.
867
868 **Supplemental file 4.** Comparison of patterning of the producer in sessile oxic co-culture (**A**) Producer
869 (Nap/Nar) shows lysis throughout biofilms and when paired with the consumer, regardless of
870 fluorescent identifier; producer shows lysis in the absence of consumer contact. (**B**) Producer (Nar)

871 shows lysis in the center of biofilm, and no significant difference compared to in the presence or
872 absence of the consumer. (**C**) Proposed model in which the Nap/Nar producer and consumer strains
873 both grow clonally until the microenvironment changes such that the producer begins to lyse. The
874 consumer acts as a sink for NO in close proximity to the producer, relieving NO toxicity and preventing
875 lysis.
876
877 **Supplemental Table 1**. Primers, plasmids, cut sites and strains used to make the mutants used in this
878 study.
879
880

Figure 1

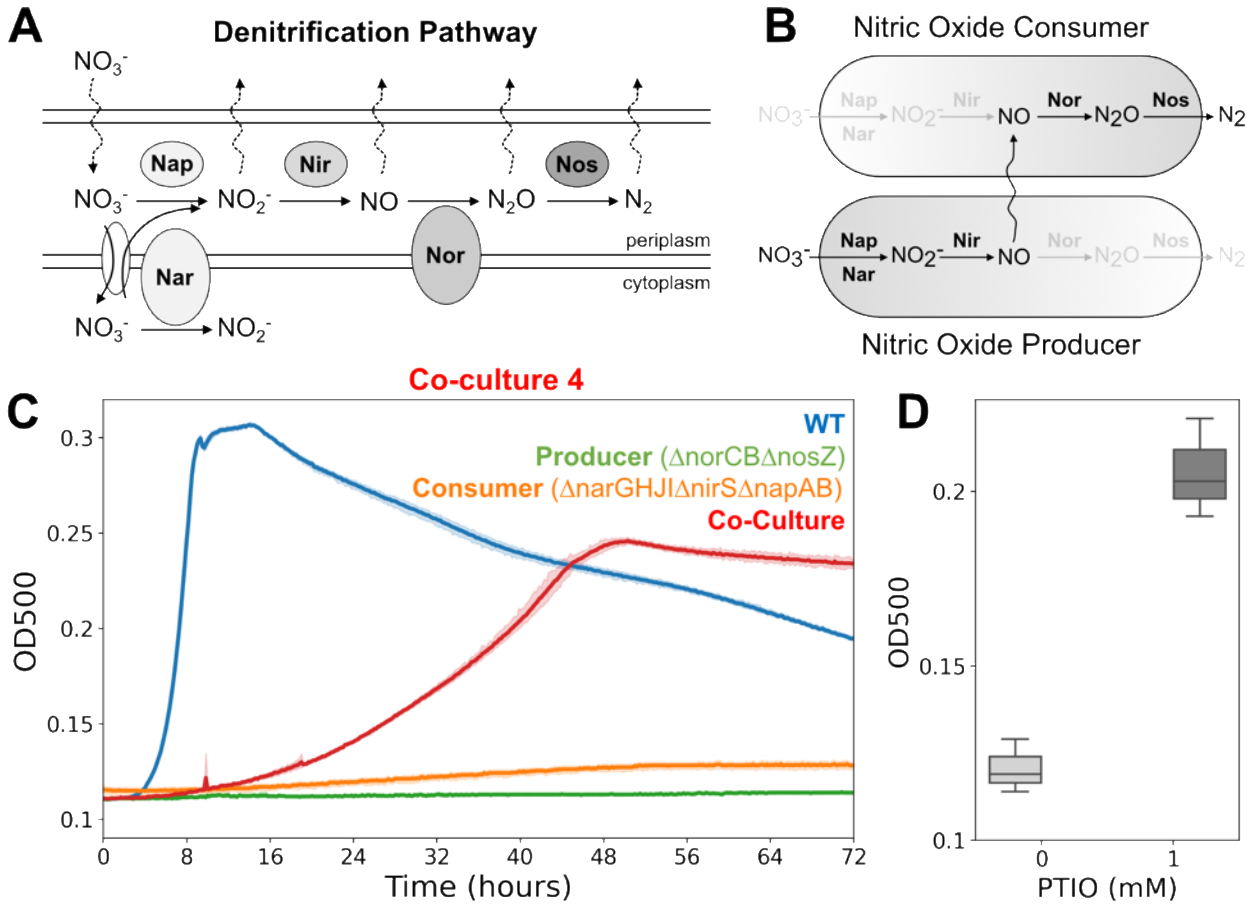

Supplementary file 1

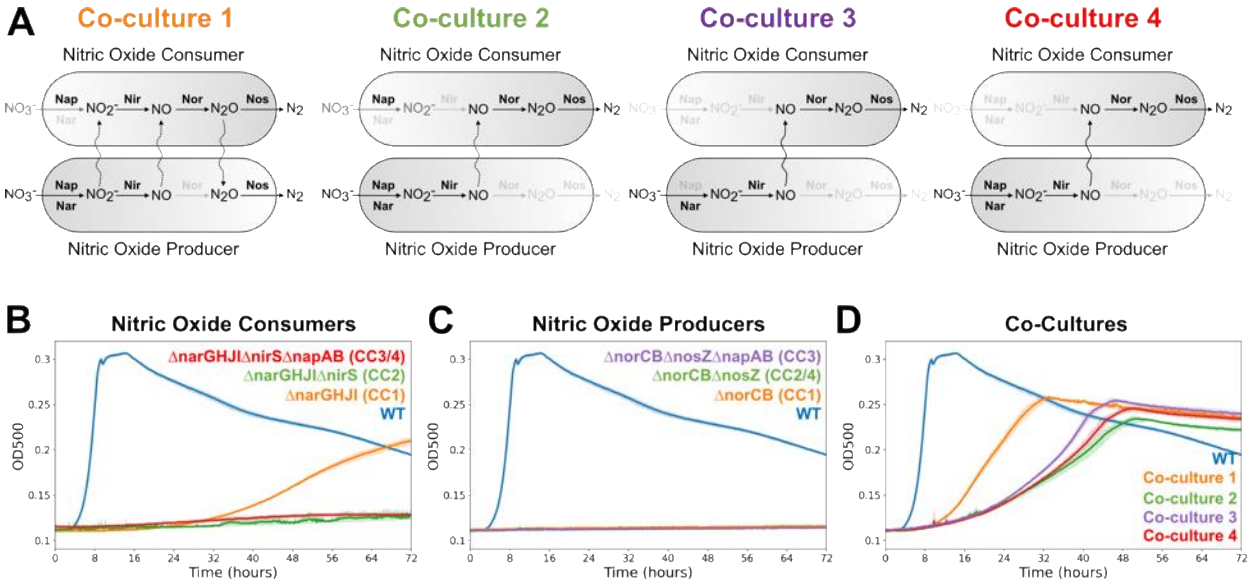

Figure 2

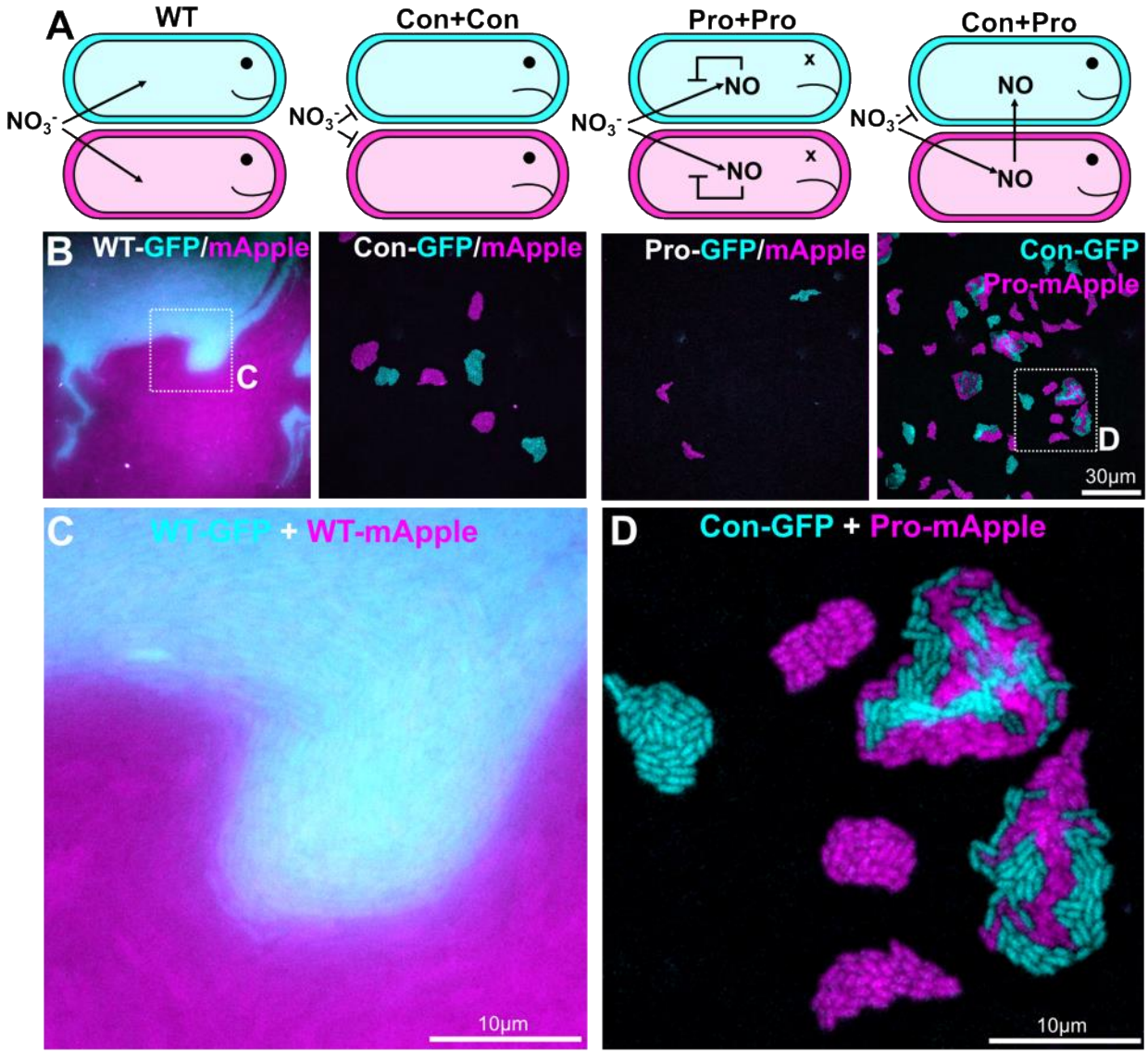

Supplementary file 2

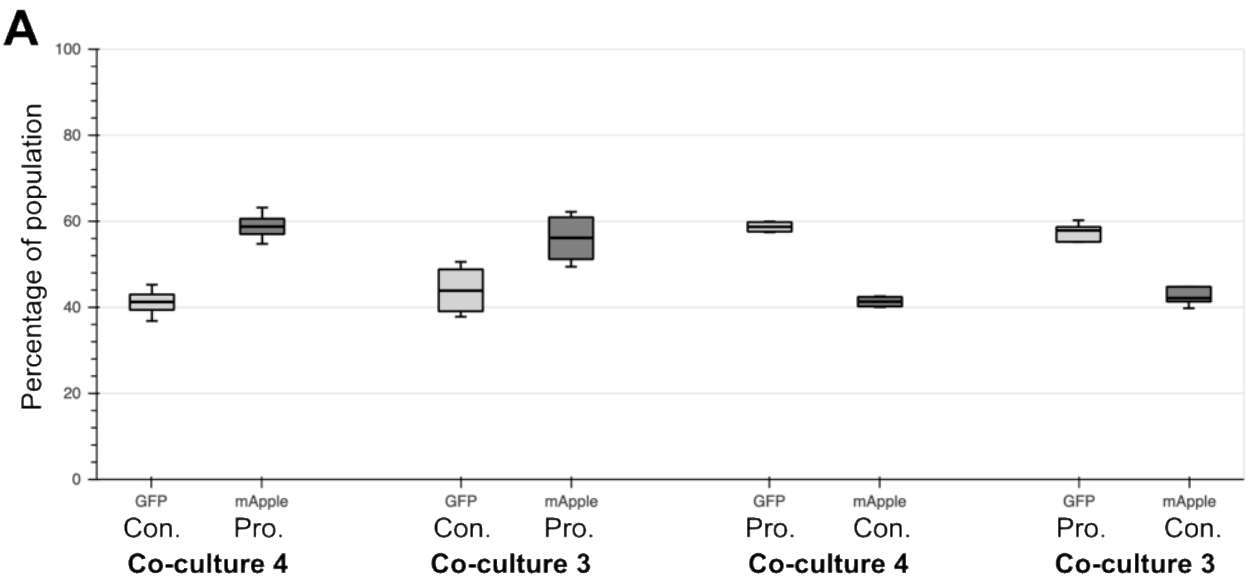

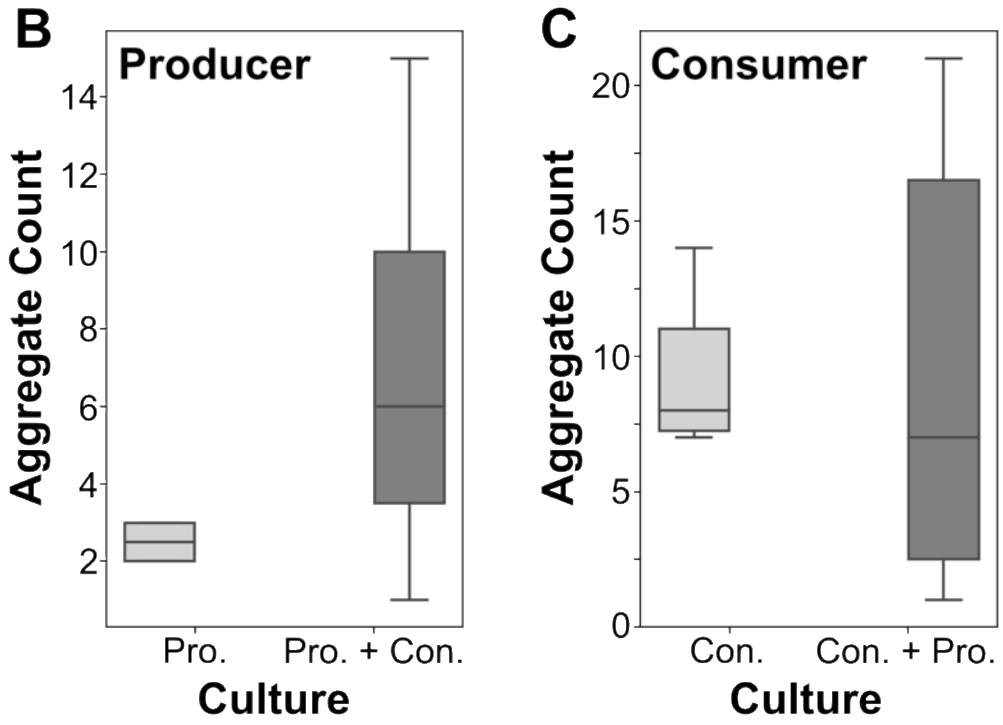

Figure 3

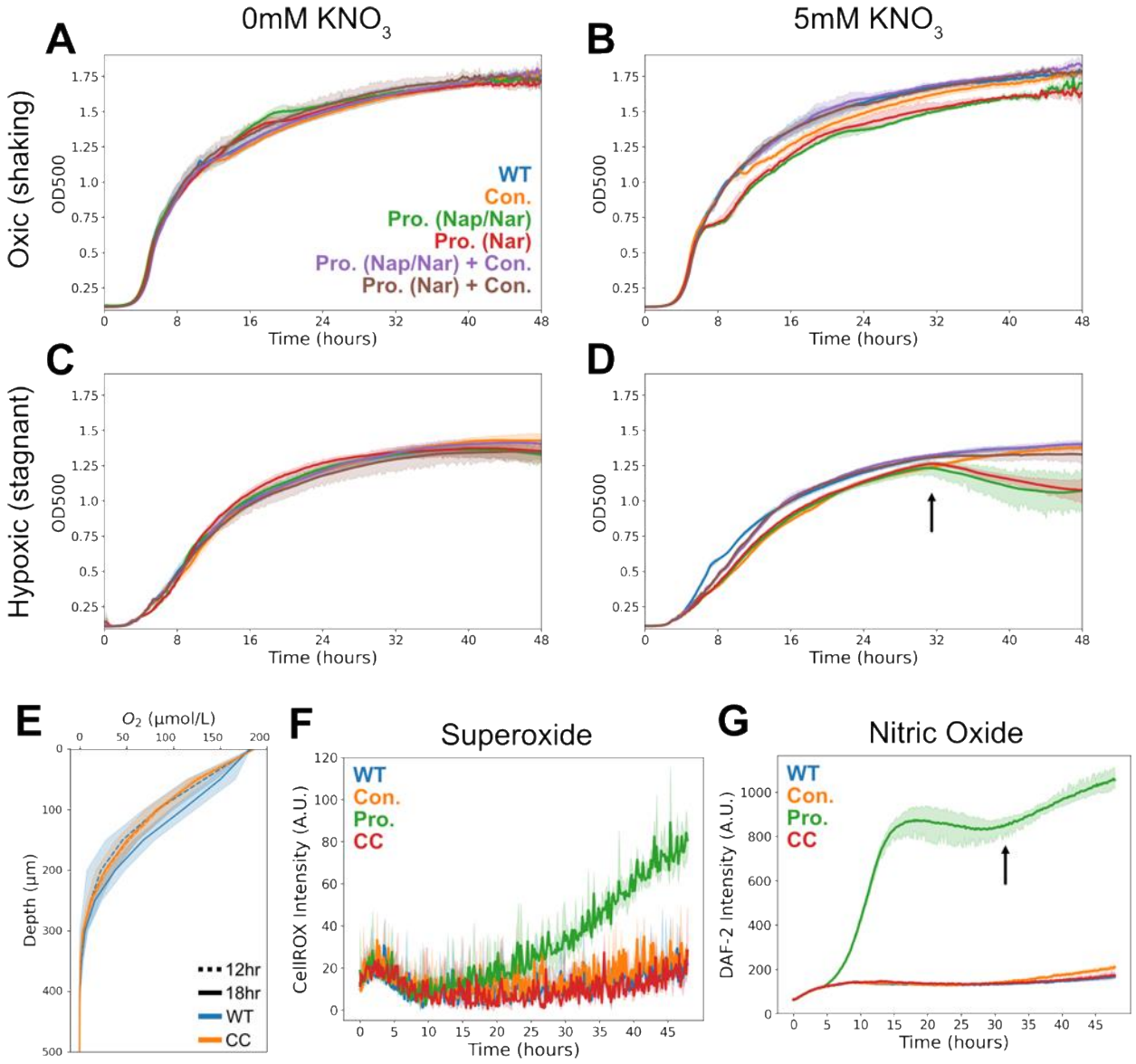

Figure 4

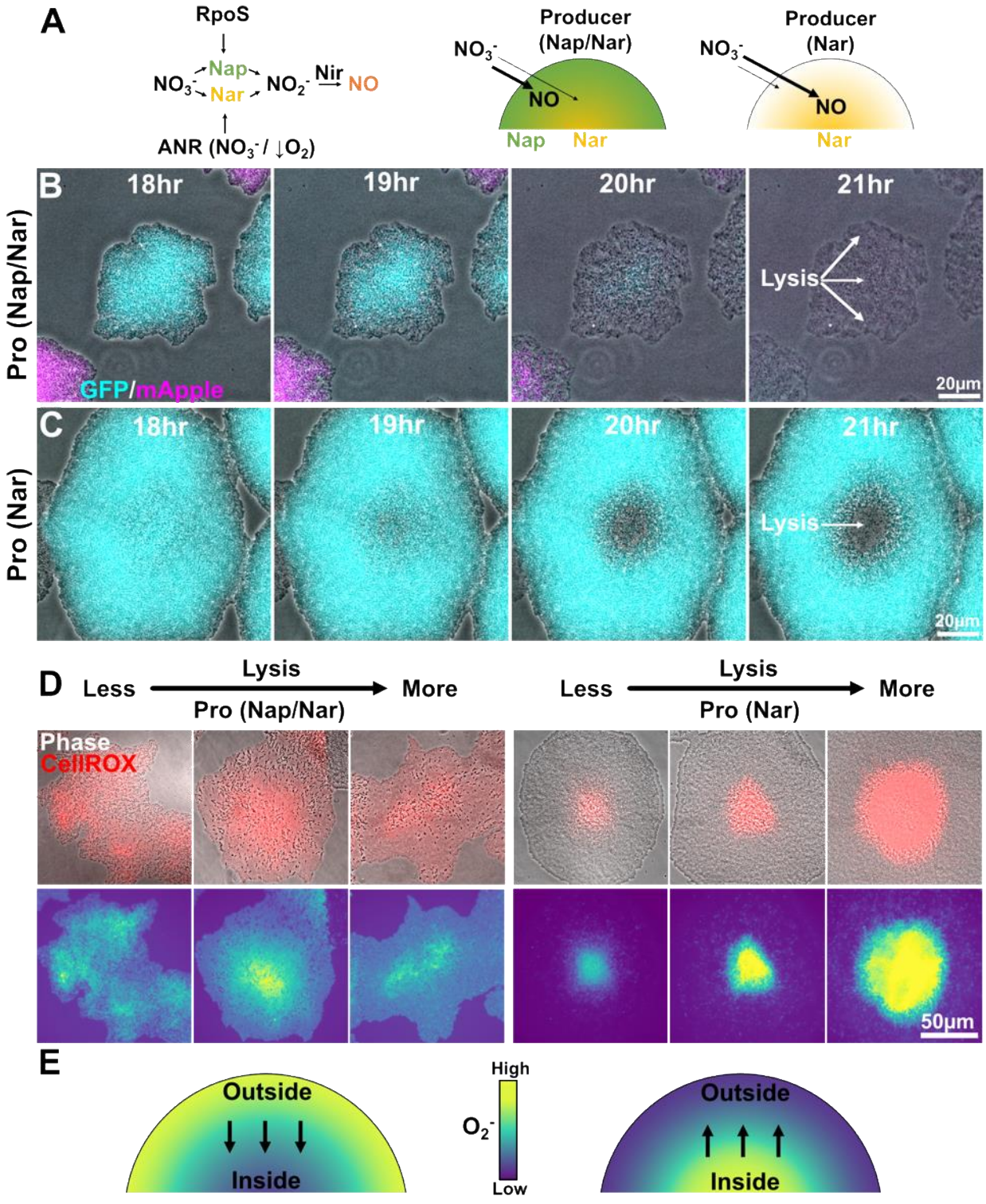

Supplementary file 3

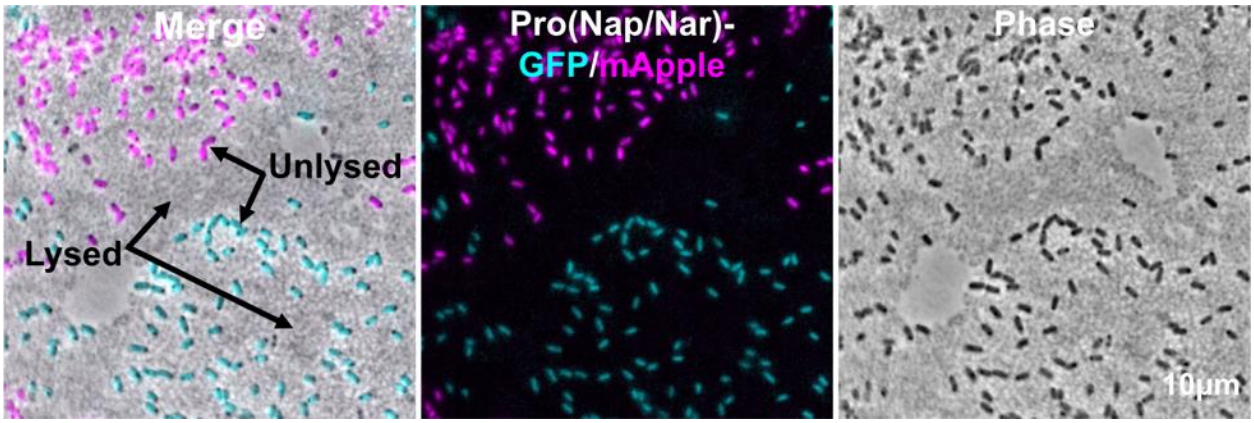

Figure 5

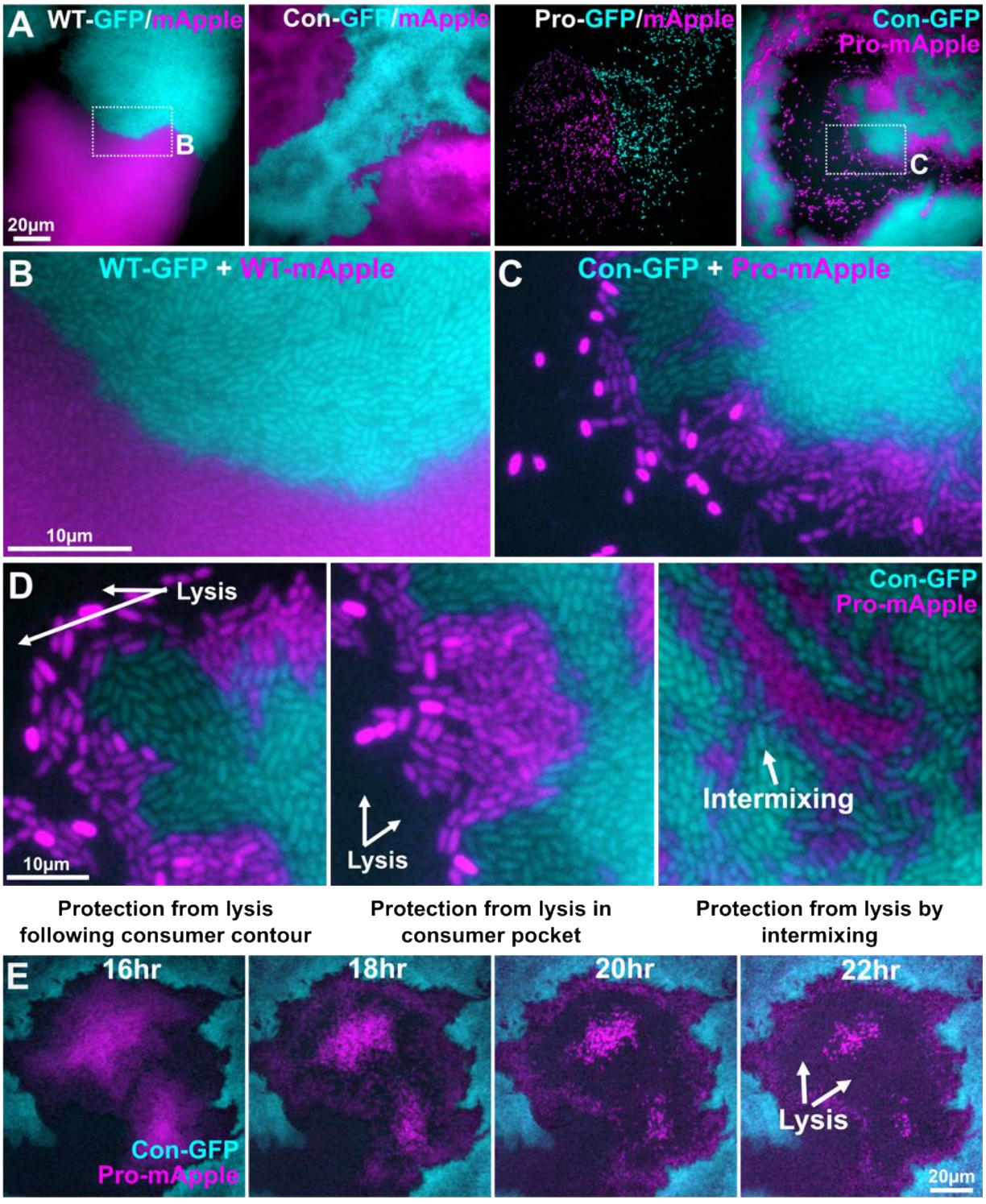

Supplementary file 4

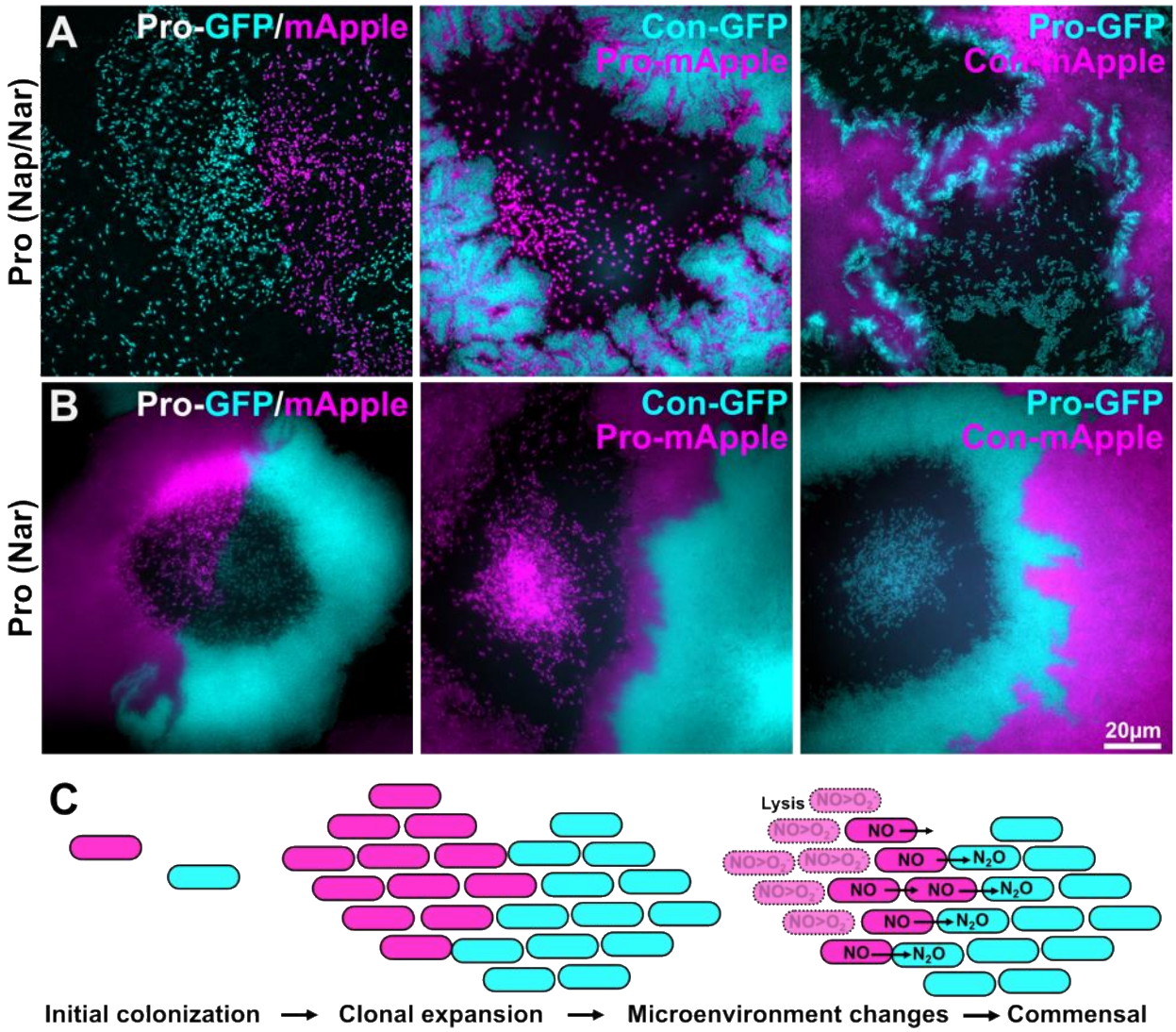

Supplementary Table 1

Deletion Construct	NarGHJI	NapAB	NirS	NorCB	NosZ
Function	Membrane bound nitrate reductase	Periplasmic nitrate reductase	Nitrite reductase	Nitric oxide reductase	Nitrous oxide reductase
Up F	TAAAACGACGGCCAGTGCCAAGCTTCTACAGTCGCCTGCATAGA	ACGACGGCCAGTGCCAAGCTTGTCGATGCGCTGGGCCAGICA	ACGACGGCCAGTGCCAAGCTTGTCGATGCGCTGGGCCAGICA	TAAAACGACGGCCAGTGCCATGATCCTCGGCTGGCTGG	ACGACGGCCAGTGCCAAGCTACGTACTTGACCTGCTGGCG
Up R	CGCGCAGGGTCTGATCTCCTCACCCGGTC	GTGCTTTCATCGCGGCCTCCCCGATTGTCTCTCGGGCGAG	GGCTCCTGAGGAGATAGACCGCGGTGCGGGGCAGC	GAAGGCCATCGGCGCCTCTGGAATGGG	GCCCTTGAGGACGACGAGTCCACTCAGCGGTCGATG
Dn F	GGAGATCAAGACCCTGCGGCGGCCGGCGTCAT	CTCGCCCGAGGAGACAATCGGGGAGGCCGCATGAAAGCACTCA	GCGTGCCCCGCACGCGGGTCGGTCTATCTCCTCAGGAGCC	AGGAGGCCGGCGATGGCCTTCGCGTCGAG	CATCGACCGGCGCTGAGTGGACTCGTGTCGTCCTCAAGGGC
Dn R	CATGATTACGAATTCGA GCTGCTGGCGGCGGCAGGAAGCGC	CATGATTACGAATTCGAGCTTCCTGCGACCGGGGCCCAG	CATGATTACGAATTCGAGCTTATCAGGCGACATGGAGATC	CATGATTACGAATTCGAGCTCGGGCAATCGTCCAGCG	CATGATTACGAATTCGAGCTGAGGAACTGGCCGCCCTGGA
Plasmid	pMO30	pMO30	pMO30	pMO30	pMO30
Cut Sites	HindIII, SacI	HindIII, SacI	HindIII, SacI	HindIII, SacI	HindIII, SacI
Published	Spero et al 2018	This study	This study	This study	This study

Strain name	Parent	Deletion	Function of deletion	Published
PA14 (WT)	PA14	NA	NA	NA
ΔnarGHJI	PA14	NarGHJI	Membrane nitrate reductase	Spero et al 2018
ΔnorCB	PA14	NorCB	Nitric oxide reductase	This study
ΔnirS	PA14	NirS	Nitrite reductase	This study
ΔnarGHJIΔnirS	ΔnirS	NarGHJI	Membrane bound nitrate reductase, nitrite reductase	This study
ΔnorCBΔnosZ	ΔnorCB	NosZ	Nitric oxide reductase, nitrous oxide reductase	This study
ΔnarGHJIΔnirSΔnapAB	ΔnarGHJIΔnirS	NapAB	Membrane nitrate reductase, nitrite reductase, periplasmic nitrate reductase	This study
ΔnorCBΔnosZΔnapAB	ΔnorCBΔnosZ	NapAB	Nitric oxide reductase, nitrous oxide reductase, periplasmic nitrate reductase	This study